

Reconsidering the energy efficiency of spiking neural networks

Zhanglu YAN*, Zhenyu Bai*,†, Weng-Fai Wong

School of Computing, National University of Singapore

zhangluyan@comp.nus.edu.sg; zhenyu.bai@nus.edu.sg, wongwf@nus.edu.sg

Abstract

Spiking neural networks (SNNs) are generally regarded as more energy-efficient because they do not use multiplications. However, most SNN works only consider the counting of additions to evaluate energy consumption, neglecting other overheads such as memory accesses and data movement operations. This oversight can lead to a misleading perception of efficiency, especially when state-of-the-art SNN accelerators operate with very small time window sizes. In this paper, we present a detailed comparison of the energy consumption of artificial neural networks (ANNs) and SNNs from a hardware perspective. We provide accurate formulas for energy consumption based on classical multi-level memory hierarchy architectures, commonly used neuromorphic dataflow architectures, and our proposed improved spatial-dataflow architecture. Our research demonstrates that to achieve comparable accuracy and greater energy efficiency than ANNs, SNNs require strict limitations on both time window size T and sparsity s . For instance, with the VGG16 model and a fixed T of 6, the neuron sparsity rate must exceed 93% to ensure energy efficiency across most architectures. Inspired by our findings, we explore strategies to enhance energy efficiency by increasing sparsity. We introduce two regularization terms during training that constrain weights and activations, effectively boosting the sparsity rate. Our experiments on the CIFAR-10 dataset, using T of 6, show that our SNNs consume 69% of the energy used by optimized ANNs on spatial-dataflow architectures, while maintaining an SNN accuracy of 94.18%. This framework, developed using PyTorch, is publicly available for use and further research.

Introduction

Edge computing has gained prominence by processing data locally instead of relying on cloud servers, thus conserving battery life and enabling applications in environments where signal transmission is constrained (Chen et al. 2021; Jiang et al. 2020; Rashid et al. 2022). By replacing multiplications with additions to enhance local computation, *spiking neural networks* (SNNs) have acquired a reputation for energy efficiency (Yan et al. 2024). However, recently there are some researchers have questioned the energy efficiency of SNNs

by highlighting the computational overheads, such as memory accesses and data movements. This contrast poses critical questions that we aim to address in this paper: are SNNs truly more energy-efficient than ANNs, and what are the factors that determine the energy efficiency of SNNs?

In fact, the comparison of energy consumption between ANNs and SNNs is very complex and varies greatly depending on the specific architectures, mapping algorithms, and network structures used. Moreover, ANNs can also be optimized to leverage parameter reuse and exploit sparsity. A fair comparison should involve an ideally optimized ANN. Only if SNNs surpass these optimized ANNs in performance, taking into account all hardware overheads, can we confidently declare SNNs are energy-efficient.

In this paper, we conduct a detailed analysis of the energy consumption of ANNs and SNNs across various architectures. On classical *multi-level memory hierarchy architectures* like GPUs, shown in Figure 1a, we assume that ANNs have optimal sparsity and weight reuse to minimize the DRAM energy, serving as the benchmark for their most efficient energy use. Then, we assess SNNs under specific conditions of time window size and sparsity to determine when they surpass this benchmark on the same system. For dataflow architecture, *neuromorphic dataflow architectures* (Figure 1b I) reduce SNN energy by substituting activation read and storage with network-on-chip(NOC) data movement. However, direct comparisons with ANNs are challenging because these architectures are designed for SNNs to exploit bit-level sparse spike patterns. Thus, we keep exploring the *spatial-dataflow architecture*(Figure 1b II), which utilizes a mesh NOC design that prioritizes connections between neighboring processing elements to eliminate long-distance data transfers. We use a sparsity-aware mapping strategy that minimizes router impact, enabling both ANNs and SNNs to operate on this architecture. We then make a fair comparison of energy consumption on the dataflow architecture.

For the widely used VGG16 model, our findings indicate that stringent requirements for time window size (T) and sparsity s are necessary for SNNs to outperform ANNs in energy efficiency on both classical and spatial-dataflow Architectures. Specifically, a sparsity rate exceeding 97% is required when $T > 16$, typically at the cost of reduced accuracy for SNNs. Additionally, with a smaller T of 6, sparsity

*These authors contributed equally.

†corresponding author

Copyright © 2025, Association for the Advancement of Artificial Intelligence (www.aaai.org). All rights reserved.

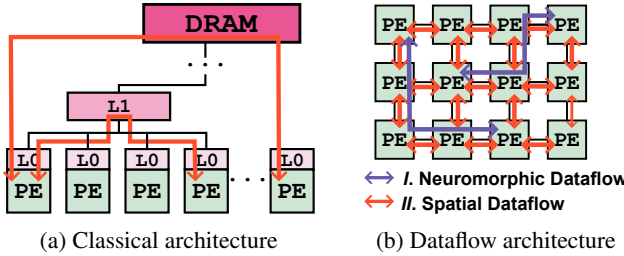


Figure 1: Comparative architectures

must surpass 93% on most architectures to realize energy savings.

Despite their potential to save energy, we find that most SNNs fail to meet the stringent requirements for true energy efficiency. To address this challenge, we introduce two regularization terms that limit weights and activations, enhancing sparsity and reducing energy consumption in SNNs. By applying these techniques to the CIFAR-10 dataset using the VGG16 model with a fixed T of 6, we can increase the sparsity rate to 94.19% and achieve an SNN accuracy of 92.76%. Consequently, our optimized SNNs now consume only 85% and 78% of the energy required by ANNs on classical and spatial-dataflow Architectures, respectively, demonstrating their superior energy efficiency.

The key contributions are summarized as follows:

- We explore the limitations of SNNs and identify two critical factors— (s) and (T) —that determine their energy efficiency. By introducing a dynamic energy consumption equation tailored for both ANNs and SNNs across various architectures, we offer specific recommendations for s and T where SNNs can achieve energy savings over ANNs in the digital domain.
- We implement two regularization terms during training to progressively increase the sparsity rate, leading to more energy-efficient SNNs. State-of-the-art energy efficiency can be achieved.
- We introduce a novel SNN design for spatial-dataflow architectures, specifically engineered to minimize data communication energy, enhancing overall efficiency.

The paper is organized as follows: Section discusses the workflow and optimization strategies for SNNs. Section compares the energy consumption of different architectures across SNNs and ANNs. In Section , we introduce two training methods that improve the sparsity and efficiency of SNNs. Finally, Section presents the enhanced energy efficiency results of our SNN models on the CIFAR-10 and CIFAR-100 datasets and compares these with prior work.

Background

SNNs use binary spike trains over a time window size of T , consisting of only 0s and 1s, to transmit information among layers. Rate-encoded SNNs encode membrane potential information through the firing rates of neurons, providing robust data representation (Stein, Gossen, and Jones 2005; Brette 2015). Commonly, integrate-and-fire (IF) model is

used to generate spikes (Eshraghian et al. 2023; Ganguly and Chakrabarti 2020; Rueckauer et al. 2017; Wu et al. 2023). In the IF model, each neuron at timestep t calculates the weighted sum of incoming spikes and biases, adds this to the membrane potential V from the previous timestep $t - 1$, and checks against a threshold θ . If exceeded, the neuron emits a spike ($s_j^l(t) = 1$) and resets the potential; otherwise, it outputs '0'.

Unlike traditional neural networks, SNNs are more hardware-friendly due to their binary nature (Yan, Zhou, and Wong 2023). However, the binary spike-based data transmission complicates the use of traditional backpropagation algorithms, which depend on partial derivatives and the chain rule. To overcome this, two primary approaches are adopted: SNN-direct training algorithms (Wu et al. 2019; Taherkhani et al. 2019) and ANN-to-SNN conversion (Yan, Zhou, and Wong 2023). The former, often relying on spike-timing-dependent plasticity (Vigneron and Martinet 2020), is hard to train and prone to overfitting. The latter approach, which we use in this study, involves training an ANN and transferring its weights to an SNN. However, direct weight transfer can lead to an accuracy drop especially when T is small. To address this, we replace ReLU function with clamp $C(x)$ and quantize $Q(x)$ functions during ANN training as described in Equation 1 and Equation 2, aligning ANN activations more closely with SNN operations.

$$C(x) = \begin{cases} 0, & x < 0 \\ x, & 0 \leq x \leq 1 \\ 1, & x > 1. \end{cases} \quad (1)$$

$$Q_T(x) = \frac{\lfloor x \cdot T \rfloor}{T} \quad (2)$$

Then, we can run the SNN inference and minimize the ANN-to-SNN conversion accuracy loss.

Energy Comparison and Analysis between ANNs and SNNs

Energy Consumption

In our study, we analyze two primary contributors to energy consumption in spiking neural networks: the energy required by computing units and the energy used for memory operations, which include both input data delivery to computing units and the movement of intermediate results. Given the highly parallel nature of current spatial architectures, developing a unified model is challenging due to variables such as the computation's mapping to compute units and the size of each unit's local memory. Effective mapping can enhance data reuse within a compute unit's local memory, leading to greater efficiency. In this section, we assess the models using a 'reuse factor' (RF), defined as the number of times a variable is reused once it is stored in local memory (SRAM).

Further, this paper discusses the architectures of SNNs in the digital domain. While the analog domain remains promising for SNNs, it is less mature in terms of product development compared to the digital domain.

Classical Architectures

Classical accelerators like GPUs, TPUs, and NPUs can be abstractly modelled as computing units situated above a multi-level memory hierarchy. The hierarchical memory system exchanges inputs, outputs, and intermediate data (Chen et al. 2020).

In the ANN model, energy consumption is outlined in Equation 3. For each neuron, weights are initially transferred from DRAM to SRAM; however, the cost associated with this transfer ($E_{R_{\text{weight}}}^{\text{DRAM}} + E_{W_{\text{weight}}}^{\text{SRAM}}$) is mitigated by reusing the weights. We specifically consider scenarios where activations and outputs for each layer are small enough to be cached within local SRAM, eliminating DRAM operations for them. This is typically feasible in CNN architectures like VGG, where the average size of layer activations is usually smaller than 18KB and can be efficiently stored in SRAM (Mascarenhas and Agarwal 2021). Then both activations and weights are accessed from local SRAM for computations.

$$E_{\text{ANN}} = N_{\text{src}} * \left(\underbrace{\frac{E_{R_{\text{weight}}}^{\text{DRAM}} + E_{W_{\text{weight}}}^{\text{SRAM}}}{RF_w}}_{\text{move weights to SRAM}} + \gamma \underbrace{(E_{\text{MAC}})}_{\text{compute}} \right) + \underbrace{\left(E_{R_{\text{input}}}^{\text{SRAM}} + E_{R_{\text{weight}}}^{\text{SRAM}} + E_{R_{\text{Output}}}^{\text{SRAM}} + E_{W_{\text{Output}}}^{\text{SRAM}} \right)}_{\text{read inputs/weights, store output to SRAM}} \quad (3)$$

, where N_{src} represents the number of source neurons that have a connection to the target neuron, and $1 - \gamma$ indicates the sparsity rate that the ANN can exploit.

The reuse factor for a convolutional layer can be expressed as:

$$RF_w = \left\lfloor \frac{H_{in} - K_h + 2P_h}{S_h} + 1 \right\rfloor * \left\lfloor \frac{W_{in} - K_w + 2P_w}{S_w} + 1 \right\rfloor \quad (4)$$

, where H_{in} and W_{in} denote the height and width of the input, respectively; K_h and K_w represent the kernel height and width; P_h and P_w specify the padding along the height and width; and S_h and S_w refer to the stride lengths in the height and width dimensions.

For SNNs, the dependency across timesteps introduces additional overhead on these accelerators. SNNs use the same weights across different timesteps but require only one bit of the input spike train per timestep. Consequently, the energy consumption per timestep in an SNN is comparable to producing a single output in an ANN. The key differences include:

- MAC are replaced by simpler ADD.
- SNNs demand higher local memory capacity to cache weights between timesteps, enhancing data reuse but requiring more memory.
- While the ANN model loads n-bit activations, SNNs load 1-bit inputs, modeled by $\frac{1}{k}$ ($k < N$ because finer granularity of data movement leads to lower efficiency).
- SNNs use different activation functions from ANNs and SNNs leverage finer sparsity.

Thus, we can present energy of SNNs as follows:

$$E_{\text{SNN}} = N_{\text{src}} * T * \left(\underbrace{\frac{E_{R_{\text{weight}}}^{\text{DRAM}} + E_{W_{\text{weight}}}^{\text{SRAM}}}{RF'_w}}_{\text{move weights to SRAM}} + (1 - s) * \underbrace{(E_{\text{ADD}})}_{\text{compute}} \right) + \underbrace{\left(E_{R_{\text{input}}}^{\text{SRAM}} + E_{R_{\text{weight}}}^{\text{SRAM}} + E_{R_{\text{Output}}}^{\text{SRAM}} + E_{W_{\text{Output}}}^{\text{SRAM}} \right)}_{\text{read inputs/weights, storing output}} + T * \underbrace{\left(E_{R_{\text{state}}}^{\text{SRAM}} + E_{R_{\text{output}}}^{\text{SRAM}} \right)}_{\text{read membrane potential}} + \underbrace{\left(E_{\text{ADD}} + E_{\text{CMP}} \right)}_{\text{add and compare}} + \underbrace{\frac{E_{W_{\text{spike}}}^{\text{SRAM}}}{k}}_{\text{store spike}} + \underbrace{(1 - s)E_{\text{SUB}}}_{\text{firing}} + \underbrace{E_{W_{\text{state}}}^{\text{SRAM}}}_{\text{update potential}} \quad (5)$$

The reuse factor for SNNs, RF'_w , can be formulated as ranging between RF_w and $T \times RF_w$. The worst-case scenario occurs when no weight reuse between time window size is possible, requiring each time to process weights in a manner similar to ANNs, but on a per-timestep basis. In the best case, weights are effectively reused across all timesteps.

Neuromorphic Dataflow Architecture

Unlike GPUs, dataflow architectures emphasize distributed memory and on-chip data transfers among smaller compute cores, known as Processing Elements (PEs). These architectures mainly manage on-chip data transfers at a finer granularity, reducing the overhead associated with memory operations in traditional memory-centralized architectures. This design makes dataflow architectures particularly well-suited for handling SNNs, as it aligns with the network's distributed processing needs. Examples of such processors include digital neuromorphic chips, such as Intel's Loihi series and IBM's TrueNorth (Cheng et al. 2017; Lines et al. 2018). This design is characterized by the local memories of each PE and the connectivity among each pair of PEs through a NOC, as shown in Figure 2. The core idea of neuromorphic chips is to replace the cost of reading and storing activations from the memory system by data movement over the NOC. Considering the high bit-wise sparsity of SNN, the data movements are more efficient.

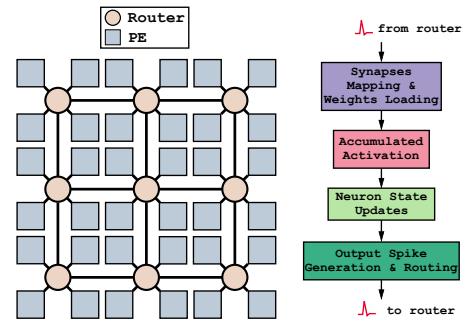


Figure 2: Classical neuromorphic architecture

Typically, multiple neurons are statically mapped to each PE. The weights of the inputs of the neuron are stored in the

PE's local memory. PE is event-triggered and works only upon the new arrival of spikes. As illustrated in Figure 2, each PE should minimally be capable of several key functions: receiving a spike from the router, retrieving the corresponding weight from local memory for the spike generator and the receiving neuron (to maximize PE utilization, several neurons are typically assigned to one PE), accumulating the voltage of the receiving neuron, updating the neuron's state, and, if the neuron spikes post-accumulation, generating an output spike packet to send back to the router. Most neuromorphic chips are optimized specifically for SNNs due to their efficient handling of sparse spike data, making the running of ANNs significantly less efficient on these platforms. Given the platform's specific design optimizations, we focus solely on running SNNs and present their energy consumption as follows:

$$\begin{aligned}
 E_{\text{SNN}} = & N_{\text{src}} * \underbrace{T * (1 - s)}_{\text{number of actual spikes}} * \underbrace{(E_{R\text{weight}}^{\text{SRAM}} + E_{\text{ADD}})}_{\text{read weight and add operations}} \\
 & + T * \underbrace{(E_{R\text{state}}^{\text{SRAM}} + E_{\text{ADD}} + E_{\text{CMP}})}_{\text{read state}} + \underbrace{(1 - s)E_{\text{SUB}}}_{\text{firing}} + \underbrace{E_{W\text{state}}^{\text{SRAM}}}_{\text{update potential}} \\
 & + N_{\text{src}} * T * (1 - s) * \underbrace{N_{\text{hop}} * E_{\text{TPHOP}}}_{\text{data movement}} \quad (6)
 \end{aligned}$$

Here, N_{hop} represents the average number of hops—or the number of routers a spike passes through—to reach its destination neuron. E_{TPHOP} denotes the energy expended per hop.

Spatial-Dataflow Architecture

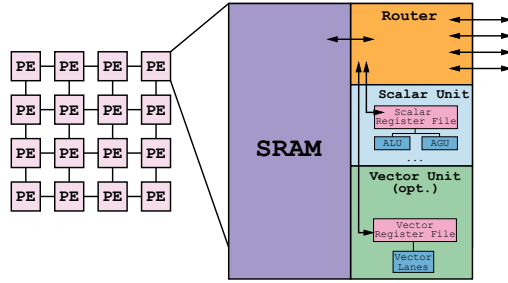


Figure 3: Spatial-dataflow architecture

In neuromorphic architecture, computation is handled efficiently, yet network costs pose significant challenges. The NOC must ensure robust connectivity, allowing each neuron from one layer to connect to any neuron in the subsequent layer. When layers have high dimensionality, data transfers between distantly located neurons become costly. Additionally, this can lead to excessive network traffic, causing congestion and necessitating increased network capacity.

However, other dataflow architectures like SambaNova, AMD AI Engine, and Tenstorrent offer alternative solutions to network cost issues. These architectures feature larger Processing Elements (PEs) equipped with local memory and specialized Instruction-Set Architectures, such as RISC-V-based or Very-Long-Instruction-Word (VLIW)-based systems. Typically, their NOC design prioritizes connections

between neighboring PEs. While any-to-any data transfer is technically possible, it is restricted, with most data transfers occurring between adjacent PEs. The key distinction between these and neuromorphic architectures lies in the enhanced capabilities of PEs—larger memory and greater computational power—and reduced capacity for long-distance data transfers.

Inspired by Gustavson's data flow (Gustavson 1978), we have developed an improved mapping design. This design efficiently maps both convolution-based and MLP-based SNNs onto these accelerators, ensuring minimal data transfers across distantly located PEs. The details of such mappings are illustrated as follows:

Figure 4 depicts the mapping process for the FC layer. During inference, constant weights, indexed by the input (x) and output (y) neurons they connect and represented as $w_{x,y}$, are preloaded into the local memory of each PE. Each PE manages a subset of these connections, with the number of input neurons it handles determined by the connectivity bandwidth among PEs. For instance, a bandwidth of 128 bits per cycle allows each PE to manage 128 input neurons. Although the number of output neurons per PE can vary, this example assumes 2 output neurons per PE. Consequently, each PE stores weights equivalent to the product of its managed input and output neurons, with the total weight size needing to fit within the PE's local memory capacity.

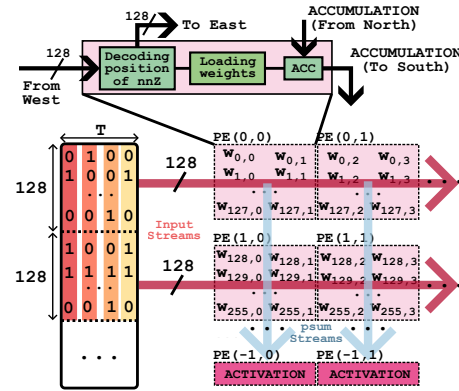


Figure 4: Mapping of fully-connected layer on spatial accelerator

In our spiking neural network model, input spikes are streamed horizontally in 128-spike packets to the PEs. Each PE decodes the positions of non-zero values, fetches the corresponding weights, and locally accumulates the weighted sums. This process computes the partial sums ($psum$) for 128 input neurons connecting to 2 output neurons. The input spikes are simultaneously transmitted to the adjacent PE on the east to process the same inputs for different output neurons. Subsequently, $psum$ values are sent vertically to the PE to the south to accumulate with additional 128 inputs. The final row of PEs aggregates these potentials to compute the output activations. This approach differs from traditional neuromorphic chip mappings by managing sparsity within the PE rather than across the NOC, enhancing scalability for larger layer dimensions. This mapping strategy can extend to

convolutional layers, where the computation of weight sums is based on kernel size. Rows share input channels across different output channels, while columns accumulate these input channels into a single output.

Consequently, the energy can be computed by:

$$E_{SNN} = N_{src} * \underbrace{T * (1 - s)}_{\text{number of actual spikes}} * \underbrace{(E_{R_{\text{weight}}}^{\text{SRAM}} + E_{\text{ADD}})}_{\text{read weight and add operations}} + \\ T * (E_{R_{\text{state}}}^{\text{SRAM}} + \underbrace{E_{\text{ADD}} + E_{\text{CMP}}}_{\text{add and compare}} + \underbrace{(1 - s)E_{\text{SUB}}}_{\text{firing}} + \underbrace{E_{W_{\text{state}}}^{\text{SRAM}}}_{\text{update potential}}) \quad (7)$$

$$E_{ANN} = N_{src} * \gamma * \underbrace{((E_{R_{\text{weight}}}^{\text{SRAM}}) + E_{\text{MAC}})}_{\text{read weight and do the MAC}} \quad (8)$$

Energy comparison on varies architectures

In this section, we derive the energy consumption for each operation, as detailed in Table 1. This analysis enables us to identify conditions, such as sparsity rate and time window size, under which SNNs achieve optimal energy efficiency.

8-bit ADD	8-bit MUL	SRAM	DRAM	NOC per hop
0.03 pj	0.2pj	20 pj	2 nj	10 pj

Table 1: Energy Consumption of different types of operation. SRAM and DRAM operations are normalized to one bit. NOC normalized to per bit per hop (Davies et al. 2018; Horowitz 2014)

Thus, within classical architectures, for an SNN to surpass the energy efficiency of an ANN, the sparsity parameter s must meet the following condition:

$$s > 1 - \frac{(80.23\gamma + \frac{2020}{RF_w}) - \frac{64.35}{N_{src}}T - \frac{2020}{RF_w}T}{(64.32 + \frac{0.03}{N_{src}})T} \quad (9)$$

Similarly, within spatial-dataflow architecture, the required sparsity s must satisfy this criterion:

$$s > 1 - \frac{20.23\gamma - \frac{40.06}{N_{src}}T}{(20.03 + \frac{0.03}{N_{src}})T} \quad (10)$$

For the neuromorphic dataflow architecture, since ANNs are not well-suited for this architecture due to its bit-level granularity of data transfer, we compare the performance of SNNs on this architecture against ANNs on two other architectures. Acknowledging that this comparison may not be entirely fair, we only detail the results in the appendix.

Using the widely implemented VGG16 network architecture as an example, we illustrate the energy efficiency breakpoint between ANNs and SNNs in Figure 5. Specifically, N_{src} and RF_w is set as the average number of source neurons and the reuse factor across all layers, respectively. For the purpose of illustrating the average-case scenario, RF'_w is equated to $(1 + T)RF/2$. In alignment with related

works (Yan et al. 2024; Dampfhofer et al. 2023), the parameter k is set at 4.66 and γ is set at 0.45. Specifically, for a time window size of $T = 6$, the energy consumption of ANNs matches that of SNNs at a sparsity rate of 0.92 and 0.93 on classical architectures and spatial-dataflow architectures. If the sparsity rate s falls below these thresholds, SNNs demonstrate greater energy efficiency on both types of architectures.

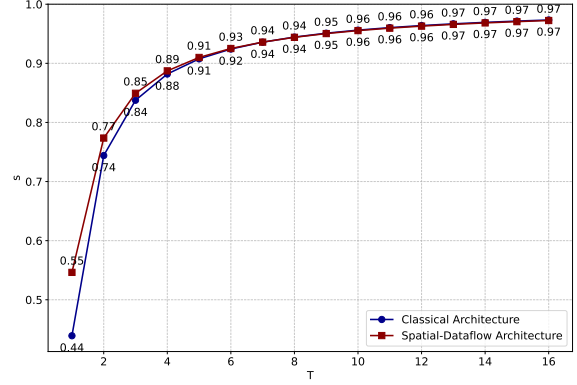


Figure 5: Energy Efficiency Breakpoints Between ANN and SNN Implementations Across Various Architectures

Additionally, for comparison, if we disregard hardware overhead, the energy consumption for ANNs can be modeled as $N_{src} \times E_{\text{MAC}}$, and for SNNs as $N_{src} \times T \times (1 - s) \times E_{\text{ADD}}$, ignoring the smaller spike energy for simplicity. Under these conditions, the sparsity s for SNNs only needs to exceed $1 - 0.23/(0.03 \times T)$ to be deemed energy-efficient. For instance, at $T = 6$, even with $s = 0$ —indicating no sparsity—SNNs would still appear more energy-efficient than ANNs. This presents a contradiction, as reality requires s to exceed 92% for actual energy savings in classical architectures. This highlights a potential misconception where SNNs may seem more energy-efficient than they truly are.

Low-sparsity and high-efficiency SNNs

To enhance the energy efficiency of SNNs relative to ANNs, our findings suggest that increasing the sparsity rate s when T is fixed. In this section, we introduce two strategies to achieve this: incorporating regularization terms specifically designed to reduce the weights and the activations, shown in Figure 6. ANN-to-SNN conversion training methods which introduced in background are used in this section.

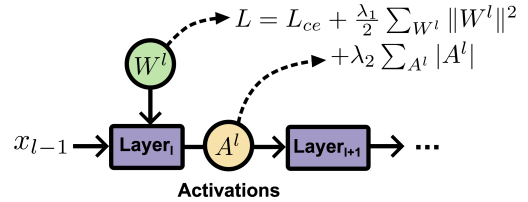


Figure 6: Sparsity-aware training algorithm

Regularization term for minimizing weight

To achieve lower spike rates, we leverage the principle that smaller synaptic weights result in reduced membrane potentials at each timestep, subsequently leading to decreased spiking activity. As detailed in Equations 11 and 12, we augment the original cross-entropy loss function, L_{ce} , with an L2 regularization term, L_w . This term is scaled by a factor, λ_1 , modulating the synaptic weights to optimize energy efficiency.

$$L_w = \frac{1}{2} \sum_{W^L l} \|W^L\|^2 \quad (11)$$

$$L = L_{ce} + \lambda_1 L_w \quad (12)$$

In exploring the trade-off between SNN accuracy and efficiency, we use the VGG16 architecture applied to the CIFAR-10 dataset as a case study. We train the network for 100 epochs with a learning rate of 1e-2 and investigate the relationship between SNN accuracy and sparsity across various time window sizes.

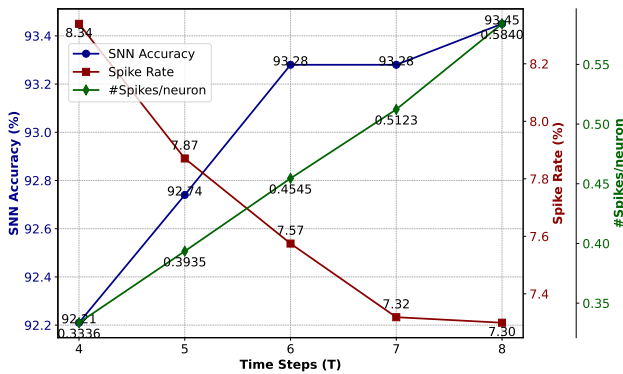


Figure 7: SNN performance with different T with VGG16 on CIFAR-10

As shown in Figure 7, the number of spikes per neuron increases when the time step is increased from 4 to 8. With a given T and s , while energy consumption also increases, there is a corresponding rise in accuracy. For further optimization in this section, we have selected $T = 6$ as the baseline, since reducing T further decreases accuracy a lot, dropping from 93.28% to 92.74%.

Subsequently, we adjust the regularization scaling factor λ_1 , testing values from 0.5 down to 0.01 to evaluate its impact on SNN accuracy and energy consumption. We identify $\lambda_1 = 0.05$ as an optimal starting point for further optimization, as it balances maintaining accuracy with reducing spike frequency. An increase in λ_1 to 0.1 results in an accuracy decrease of over 1%.

Regularization term for minimizing activations

Furthermore, by lowering activation levels during training, we can reduce spike count and enhance sparsity when converting the model to an SNN. We control the activations A^L of the convolutional layers by clamping them (see Eq 1) between 0 and 1, followed by quantization (see Eq 2),

	$\lambda_1 = 0.5$	$\lambda_1 = 0.1$	$\lambda_1 = 0.05$	$\lambda_1 = 0.01$
SNN accuracy	91.01	92.13	93.03	93.04
Sparsity rate %	94.06	93.51	92.92	92.68
#Spikes/neuron	0.3561	0.3894	0.4248	0.4392

Table 2: SNN performance with different λ_1 on CIFAR-10 with VGG16 structure and T of 6

and record the modified activations. We introduce a regularization term L_a , which sums all activations post-clamp and quantization, and integrate it into the original cross-entropy loss function, L_{ce} , to further decrease activation levels. Building on previous results, we continue to train the network using varying levels of λ_2 applied to L_a .

$$A^L = C(Q_T(A^L)) \quad (13)$$

$$L = L_{ce} + \lambda_2 \sum_l |A^L| \quad (14)$$

As demonstrated in Table 3, after training for 100 epochs, we achieved an SNN accuracy of 92.76% with a sparsity rate of 94.19% using a scaling factor of $\lambda_2 = 1 \times 10^{-6}$. Using either a larger or smaller scaling factor results in significant accuracy drops to as low as 86.41% or maintains a low sparsity rate. Consequently, we have set λ_2 at 1×10^{-6} .

	$\lambda_2 = 1e-5$	$\lambda_2 = 1e-6$	$\lambda_2 = 1e-7$	$\lambda_2 = 1e-8$
SNN accuracy	86.41	92.76	92.85	92.90
Sparsity rate %	96.35	94.19	93.68	92.96
#spikes/neuron	0.2190	0.3483	0.3793	0.4227

Table 3: SNN performance with different λ_2 on CIFAR-10 with VGG16 structure and T of 6

Results

SNN performances

The comprehensive experimental results are presented in Table 5. We employed a range of VGG network structures, from the smaller scale VGG* to VGG19, each trained with a learning rate of 5e-3 and hyper-parameters optimized as discussed in the previous section. Testing on the CIFAR-10 dataset with models VGG* and VGG16, we achieved SNN accuracies of 94.18% and 92.76%, respectively, and corresponding sparsity rates of 94.85% and 94.19%, all at a time window size of $T = 6$. Comparable outcomes are observed on the CIFAR-100 dataset, where the VGG16 model achieved an SNN accuracy of 69.44% and a sparsity rate of 93.98%. Similarly, the VGG* model reached an accuracy of 76.63% and a sparsity rate of 93.41%.

VGG-13	64*2, A, 128*2, A, 256*2, A, 512*2, A, 512*2, A
VGG-16	64*2, A, 128*2, A, 256*3, A, 512*3, A, 512*3, A
VGG-19	64*2, A, 128*2, C, 256*4, A, 512*4, A, 512*4, A
VGG-*	128*2, A, 256*2, A, 512*2, A, 1024, A

Table 4: Summary of network structures.

The final dense classifier layer is omitted from the table in all networks. The notation 'A' represents an average pooling layer.

Network	SNN accuracy%	Sparsity rate %	$\frac{E_{SNN}}{E_{ANN}}^{1/2}$	T
CIFAR-10				
VGG*	94.18	94.85	0.70/0.69	6
VGG13	91.71	95.07	0.73/0.66	6
VGG16	92.76	94.19	0.85/0.78	6
VGG19	92.31	94.42	0.86/0.75	6
CIFAR-100				
VGG*	76.63	94.31	0.75/0.76	6
VGG13	67.65	95.71	0.68/0.58	6
VGG16	69.44	93.98	0.87/0.81	6
VGG19	68.68	92.83	0.99/0.96	6

Table 5: SNN performance on CIFAR-10 and CIFAR-100; Energy efficiency ratios $\frac{E_{SNN}}{E_{ANN}}$ indicates comparisons on classical architectures ⁽¹⁾ and spatial-dataflow architectures ⁽²⁾

Accuracy-energy trade-off

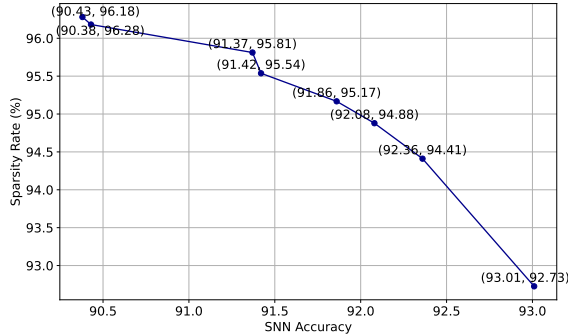


Figure 8: SNN accuracy-sparsity trade-off using VGG16 on CIFAR-10 dataset; (x,y) indicates the SNN with accuracy of x% and sparsity rate of y%

In this section, we explore the trade-off between energy consumption and sparsity using our specialized training algorithm. Using the VGG16 architecture on the CIFAR-10 dataset, we set regularization factors λ_1 at 0.05 and λ_2 at 1e-6. Over 80 epochs of training, we documented the highest accuracy SNN every 10 epochs, noting its corresponding sparsity rate. These results are presented in Figure 8, which clearly illustrates a convex relationship between accuracy and sparsity in SNNs. This pattern indicates that reductions in SNN accuracy lead to progressively smaller gains in sparsity rate. For example, a decline in SNN accuracy from 93.01% to 92.36% results in a 1.68% increase in sparsity, translating to a 2.58% increase in sparsity for each 1% drop in accuracy. In contrast, a further decrease in accuracy from 91.37% to 90.38% yields only a 0.47% improvement in sparsity, equivalent to a 0.475% increase in sparsity rate for each 1% reduction in accuracy. The trade-off between accuracy and sparsity is especially beneficial for applications where energy efficiency is more critical than perfect accuracy, allowing us to select the desired sparsity rate at a slightly reduced accuracy level.

Comparison with Related works

In our study, we benchmark the performance of our SNN against state-of-the-art SOTA SNNs from related works,

utilizing the VGG16 network structure on the CIFAR-10 dataset. A critical observation is that larger T values significantly increase the energy usage of SNNs, as maintaining high accuracy requires a sparsity rate that cannot be too low, leading to high energy consumption. For instance, the CQ+ model, with a T of 200, results in SNNs consuming 27.05 and 41.60 times more energy than ANNs on two different platforms. Similarly, models like RMP-SNN and TCS-SNN, with a slightly lower T of 64, still show SNNs using over ten times the energy of ANNs. However, lower time window size offers the potential for energy savings in SNNs with high sparsity rate. For instance, the DIET-SNN model with a T of 5 and a sparsity rate of 92.2% marginally outperforms ANNs in energy efficiency, achieving energy ratios of 0.90 and 0.87 on respective platforms. Our approach further enhances this efficiency by adjusting the loss function to restrict weights and activations, thereby increasing the sparsity rate. Consequently, our SNN, utilizing the same VGG16 architecture, achieves the lowest energy consumption—only 0.85 and 0.78 times that of ANNs on the respective platforms—while maintaining comparable accuracy.

	Accuracy%	s%	T	$\frac{E_{SNN}}{E_{ANN}}^{1/2}$	$\frac{E_{SNN}}{E_{ANN}}^2$
TCS-SNN (Han and Roy 2020)	92.79	90.5	64	9.05	13.50
RMP-SNN (Han, Srin, and Roy 2020)	90.35	91	64	8.59	12.79
DIET-SNN (Rathi and Roy 2023)	92.70	92.2	5	0.90	0.87
CQ+ SNN (Yan, Zhou, and Wong 2023)	91.45	90.63	200	27.05	41.60
VR-SNN (Yan, Zhou, and Wong 2022)	93.28	92.33	6	1.01	1.02
Ours	92.76	94.19	6	0.85	0.78

Table 6: SNN Performance Using VGG-16 on CIFAR-10 Across Studies

Conclusion

In this study, we analyze and quantify the energy consumption of ANNs and SNNs across classical, neuromorphic-dataflow, and spatial-dataflow architectures. We find that SNNs often present misleading energy savings due to overlooked hardware overhead. Energy efficiency in SNNs is only achieved under stringent conditions. For example, taking VGG16 as a case study, with a time window of $T = 6$, the sparsity rate must be at least 93% to make SNN energy efficient than ANN in most architectures, and a higher time window size makes this condition even more stringent. We hope our research can provide SNN peoples with a benchmark to show under what conditions and in which architectures SNNs are truly energy-efficient and worth pursuing. Additionally, by integrating specific regularization techniques, we achieve SNNs with a sparsity of 94.19% on the CIFAR-10 dataset with VGG16 network structure, reducing energy use to 0.85 and 0.78 times that of the best-case ANN on classical GPU-like and spatial-dataflow architectures while maintaining 92.76% accuracy. We believe our results will prompt the SNN community to prioritize true energy efficiency and foster further advancements in the field.

References

Brette, R. 2015. Philosophy of the spike: rate-based vs. spike-based theories of the brain. *Frontiers in systems neuroscience*, 9: 151.

Chen, S.; Li, Q.; Zhou, M.; and Abusorrah, A. 2021. Recent advances in collaborative scheduling of computing tasks in an edge computing paradigm. *Sensors*, 21(3): 779.

Chen, Y.; Xie, Y.; Song, L.; Chen, F.; and Tang, T. 2020. A survey of accelerator architectures for deep neural networks. *Engineering*, 6(3): 264–274.

Cheng, H.-P.; Wen, W.; Wu, C.; Li, S.; Li, H. H.; and Chen, Y. 2017. Understanding the design of IBM neurosynaptic system and its tradeoffs: A user perspective. In *Design, Automation & Test in Europe Conference & Exhibition (DATE), 2017*, 139–144. IEEE.

Dampfhofer, M.; Mesquida, T.; Valentian, A.; and Anghel, L. 2023. Are SNNs Really More Energy-Efficient Than ANNs? an In-Depth Hardware-Aware Study. *IEEE Transactions on Emerging Topics in Computational Intelligence*, 7(3): 731–741.

Davies, M.; Srinivasa, N.; Lin, T.-H.; Chinya, G.; Cao, Y.; Choday, S. H.; Dimou, G.; Joshi, P.; Imam, N.; Jain, S.; et al. 2018. Loihi: A neuromorphic manycore processor with on-chip learning. *Ieee Micro*, 38(1): 82–99.

Eshraghian, J. K.; Ward, M.; Neftci, E. O.; Wang, X.; Lenz, G.; Dwivedi, G.; Bennamoun, M.; Jeong, D. S.; and Lu, W. D. 2023. Training spiking neural networks using lessons from deep learning. *Proceedings of the IEEE*.

Ganguly, C.; and Chakrabarti, S. 2020. A discrete time framework for spike transfer process in a cortical neuron with asynchronous epsp, ipsp, and variable threshold. *IEEE Transactions on Neural Systems and Rehabilitation Engineering*, 28(4): 772–781.

Gustavson, F. G. 1978. Two fast algorithms for sparse matrices: Multiplication and permuted transposition. *ACM Transactions on Mathematical Software (TOMS)*, 4(3): 250–269.

Han, B.; and Roy, K. 2020. Deep spiking neural network: Energy efficiency through time based coding. In *European conference on computer vision*, 388–404. Springer.

Han, B.; Srin, G.; and Roy, K. 2020. Rmp-snn: Residual membrane potential neuron for enabling deeper high-accuracy and low-latency spiking neural network. In *Proceedings of the IEEE/CVF conference on computer vision and pattern recognition*, 13558–13567.

Horowitz, M. 2014. 1.1 Computing’s energy problem (and what we can do about it). In *2014 IEEE International Solid-State Circuits Conference Digest of Technical Papers (ISSCC)*, 10–14.

Jiang, C.; Fan, T.; Gao, H.; Shi, W.; Liu, L.; Cérin, C.; and Wan, J. 2020. Energy aware edge computing: A survey. *Computer Communications*, 151: 556–580.

Lines, A.; Joshi, P.; Liu, R.; McCoy, S.; Tse, J.; Weng, Y.-H.; and Davies, M. 2018. Loihi asynchronous neuromorphic research chip. *Energy*, 10(15): 10–1109.

Mascarenhas, S.; and Agarwal, M. 2021. A comparison between VGG16, VGG19 and ResNet50 architecture frameworks for Image Classification. In *2021 International conference on disruptive technologies for multi-disciplinary research and applications (CENTCON)*, volume 1, 96–99. IEEE.

Rashid, N.; Demirel, B. U.; Odema, M.; and Al Faruque, M. A. 2022. Template matching based early exit cnn for energy-efficient myocardial infarction detection on low-power wearable devices. *Proceedings of the ACM on Interactive, Mobile, Wearable and Ubiquitous Technologies*, 6(2): 1–22.

Rathi, N.; and Roy, K. 2023. DIET-SNN: A Low-Latency Spiking Neural Network With Direct Input Encoding and Leakage and Threshold Optimization. *IEEE Transactions on Neural Networks and Learning Systems*, 34(6): 3174–3182.

Rueckauer, B.; Lungu, I.-A.; Hu, Y.; Pfeiffer, M.; and Liu, S.-C. 2017. Conversion of continuous-valued deep networks to efficient event-driven networks for image classification. *Frontiers in Neuroscience*, 11: 682.

Stein, R. B.; Gossen, E. R.; and Jones, K. E. 2005. Neuronal variability: noise or part of the signal? *Nature Reviews Neuroscience*, 6(5): 389–397.

Taherkhani, A.; Belatreche, A.; Li, Y.; Cosma, G.; Maguire, L.; and Mcginnity, T. 2019. A review of learning in biologically plausible spiking neural networks. *Neural Networks*, 122.

Vigneron, A.; and Martinet, J. 2020. A critical survey of STDP in Spiking Neural Networks for Pattern Recognition (Preprint).

Wu, X.; Zhao, Y.; Song, Y.; Jiang, Y.; Bai, Y.; Li, X.; Zhou, Y.; Yang, X.; and Hao, Q. 2023. Dynamic threshold integrate and fire neuron model for low latency spiking neural networks. *Neurocomputing*, 544: 126247.

Wu, Y.; Deng, L.; Li, G.; Zhu, J.; Xie, Y.; and Shi, L. 2019. Direct training for spiking neural networks: Faster, larger, better. In *Proceedings of the AAAI Conference on Artificial Intelligence*, volume 33, 1311–1318.

Yan, Z.; Bai, Z.; Mitra, T.; and Wong, W.-F. 2024. SparrowSNN: A Hardware/software Co-design for Energy Efficient ECG Classification. *arXiv preprint arXiv:2406.06543*.

Yan, Z.; Zhou, J.; and Wong, W.-F. 2022. Low Latency Conversion of Artificial Neural Network Models to Rate-encoded Spiking Neural Networks. *arXiv preprint arXiv:2211.08410*.

Yan, Z.; Zhou, J.; and Wong, W.-F. 2023. CQ⁺ Training: Minimizing Accuracy Loss in Conversion From Convolutional Neural Networks to Spiking Neural Networks. *IEEE Transactions on Pattern Analysis and Machine Intelligence*, 45(10): 11600–11611.

Reproducibility Checklist

This paper:

- Includes a conceptual outline and/or pseudocode description of AI methods introduced (yes)
- Clearly delineates statements that are opinions, hypothesis, and speculation from objective facts and results (yes)
- Provides well marked pedagogical references for less-familiar readers to gain background necessary to replicate the paper (yes)

Does this paper make theoretical contributions? (yes)

If yes, please complete the list below.

- All assumptions and restrictions are stated clearly and formally. (yes)
- All novel claims are stated formally (e.g., in theorem statements). (yes)
- Proofs of all novel claims are included. (yes)
- Proof sketches or intuitions are given for complex and/or novel results. (yes)
- Appropriate citations to theoretical tools used are given. (yes)
- All theoretical claims are demonstrated empirically to hold. (yes)
- All experimental code used to eliminate or disprove claims is included. (yes)

Does this paper rely on one or more datasets? (yes)

If yes, please complete the list below.

- A motivation is given for why the experiments are conducted on the selected datasets (yes)
- All novel datasets introduced in this paper are included in a data appendix. (yes)
- All novel datasets introduced in this paper will be made publicly available upon publication of the paper with a license that allows free usage for research purposes. (yes)
- All datasets drawn from the existing literature (potentially including authors' own previously published work) are accompanied by appropriate citations. (yes)
- All datasets drawn from the existing literature (potentially including authors' own previously published work) are publicly available. (yes)
- All datasets that are not publicly available are described in detail, with explanation why publicly available alternatives are not scientifically satisfying. (yes)

Does this paper include computational experiments? (yes)

If yes, please complete the list below.

- Any code required for pre-processing data is included in the appendix. (yes)
- All source code required for conducting and analyzing the experiments is included in a code appendix. (yes)
- All source code required for conducting and analyzing the experiments will be made publicly available upon publication of the paper with a license that allows free usage for research purposes. (yes)

- All source code implementing new methods have comments detailing the implementation, with references to the paper where each step comes from (yes)
- If an algorithm depends on randomness, then the method used for setting seeds is described in a way sufficient to allow replication of results. (yes)
- This paper specifies the computing infrastructure used for running experiments (hardware and software), including GPU/CPU models; amount of memory; operating system; names and versions of relevant software libraries and frameworks. (yes)
- This paper formally describes evaluation metrics used and explains the motivation for choosing these metrics. (yes)
- This paper states the number of algorithm runs used to compute each reported result. (yes)
- Analysis of experiments goes beyond single-dimensional summaries of performance (e.g., average; median) to include measures of variation, confidence, or other distributional information. (yes)
- The significance of any improvement or decrease in performance is judged using appropriate statistical tests (e.g., Wilcoxon signed-rank). (yes)
- This paper lists all final (hyper-)parameters used for each model/algorithm in the paper's experiments. (yes)
- This paper states the number and range of values tried per (hyper-) parameter during development of the paper, along with the criterion used for selecting the final parameter setting. (yes)

Appendix

Experiment Setup

In this study, training was conducted using CUDA-accelerated PyTorch version 1.12.1+cu116. on a system with an AMD EPYC 7763 64-Core Processor, 1000GB of DRAM, and dual NVIDIA A100 GPUs. The system operated on Linux 5.15.0-86-generic x86_64.

Comparison on neuromorphic dataflow architecture

Due to the limitations of the neuromorphic dataflow architecture, where routers are designed to transmit binary signals, running ANNs is not feasible, making an apple-to-apple comparison with this architecture impossible. Consequently, most related works recommend comparisons with ANNs on classical architectures. However, in our paper, we present the energy efficiency breakpoints between ANNs and SNNs for both classical and spatial-dataflow architectures in Figure 9. Furthermore, the actual number of hops required for communication heavily depends on the neuron mapping across the network. For a chip typically sized 3x8, this can vary between 0 to 23 hops. For our analysis, we use an empirical average of 6 hops. We detail this relationship in the equation provided and illustrate it in the accompanying figure.

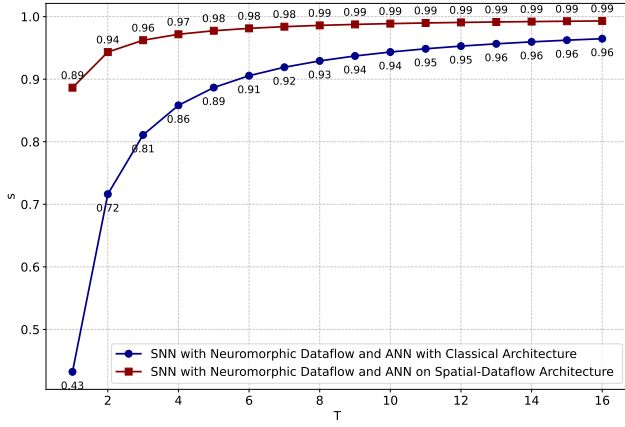


Figure 9: Energy Efficiency Breakpoints Between ANN across Various Architectures and SNN Implementations on Neuromorphic Dataflow Architecture

For SNN with neuromorphic dataflow and ANN with Classical Architecture:

$$s > 1 - \frac{80.23\gamma + \frac{2020}{RF_w} - \frac{40.06}{N_{src}}T}{(20.03 + \frac{0.03}{N_{src}} + 10N_{hop})T} \quad (15)$$

Similarly, SNN with neuromorphic dataflow and ANN with spatial-dataflow architecture:

$$s > 1 - \frac{20.23\gamma - \frac{40.06}{N_{src}}T}{(20.03 + \frac{0.03}{N_{src}} + 10N_{hop})T} \quad (16)$$